# NOVEL ORGANOSULFUR CATHODE MATERIALS FOR ADVANCED LITHIUM BATTERIES

A Thesis

Submitted to the Faculty

of

Purdue University

by

Michaela Elaine Bell

In Partial Fulfillment of the

Requirements for the Degree

of

Masters of Science in Mechanical Engineering

May 2018

Purdue University

Indianapolis, Indiana

# THE PURDUE UNIVERSITY GRADUATE SCHOOL
# STATEMENT OF COMMITTEE APPROVAL

Dr. Yongzhu Fu

Department of Mechanical and Energy Engineering

Dr. Jong Eun Ryu

Department of Mechanical and Energy Engineering

Dr. Likun Zhu

Department of Mechanical and Energy Engineering

**Approved by:**

Dr. Sohel Anwar

Chair of the Graduate Program

Dedicated to Ian, my constant.

# ACKNOWLEDGMENTS

I would like to thank my parents, Mike and Sherri Bell, for teaching me how to work hard. I'd like to thank Sherri Campbell for always knowing what to say when I'm stressed and for keeping me on track. A big thanks to Reyn Croghan for sharing in the stress of graduate school and making sure that we both relaxed and had fun. I cannot thank Ian Croghan enough for all that he has taught me about trying my best and being confident in my work.

I am thankful for Dr. Yongzhu Fu for giving me the opportunity to work alongside him and to learn from his extensive knowledge of renewable energy storage. I would like to thank Dr. Jong Eun Ryu for acting as a member of my graduate committee and for exposing me to the newest flexible electronics technology. I am so appreciative of Dr. Likun Zhu for his time and effort to be a member of my graduate committee and for his insight into lithium ion battery research.

I extend my greatest thanks to Amruth Bhargav, who spent countless hours working with me in the lab. Thank you for training me in handling chemicals and teaching my what detailed research involves. In addition to Amruth, I would like to extend my gratitude to Yi Cui, Dr. Wei Guo and Tianyi Li for making sure that our lab environment was a fun and exciting place to spend time.

TABLE OF CONTENTS

Page

# LIST OF FIGURES

Figure Page

# ABSTRACT

Bell, Michaela Elaine. M.S.M.E., Purdue University, May 2018. Novel Organosulfur Cathode Materials for Advanced Lithium Batteries. Major Professor: Yongzhu Fu.

Recent innovations in portable electronics, electric vehicles and power generation by wind and solar have expanded the need for efficient battery storage. Lithium-ion batteries have been the frontline contender of battery storage yet are not able to match current demands. Alternatively, lithium-sulfur batteries are a promising technology to match the consumer demands. Elemental sulfur cathodes incur a variety of problems during cycling including the dissolution of intermediate lithium polysulfides, an undesirable volume change ($\sim 80\%$) when completely reduced and a high dependence on liquid electrolyte, which quickly degrades the cell's available energy density. Due to these problems, the high theoretical capacity and energy density of lithium sulfur cells are unattainable. In this work, A new class of phenyl polysulfides, $C_6H_5S_xC_6H_5 (4 \leq x \leq 6)$, are developed as liquid sulfur containing cathode materials. This technology was taken a step further to fulfill and emerging need for flexible electronics in technology. Phenyl tetrasulfide ($C_6H_5S_4C_6H_5$) was polymerized to form a high energy density battery with acute mobility. Lithium half-cell testing shows that phenyl hexasulfide ($C_6H_5S_6C_6H_5$) can provide a specific capacity of $650\, mA\, h\, g^{-1}$ and capacity retention of 80% through 500 cycles at 1C rate along with superlative performance up to 10C. Furthermore, $1,302\, W\, h\, kg^{-1}$ and $1,720\, W\, h\, L^{-1}$ are achievable at a low electrolyte/active material ratio. Electrochemical testing of polymer phenyl tetrasulfide reveals high specific capacities of $634\, mA\, h\, g^{-1}$ at 1C, while reaching $600\, mA\, h\, g^{-1}$ upon mechanical strain testing. This work introduces novel cathode materials for lithium-sulfur batteries and provides a new direction for the development of alternative high-capacity flexible cathode materials.

# 1. INTRODUCTION

Fossil fuels have driven the progress of the industrial revolution since its conception. It accounts for 86% of global energy use, with the remaining 14% attributed to renewable energy sources. [1] Wind and solar energy developments are becoming more widespread as stand-alone alternatives to energy generation. Inevitable fluctuations in energy output from natural sources has disrupted the stability of the grid. A clever energy storage solution is key to the longevity of renewable resources. The finite reservoirs of oil, gas and coal in addition to the increasing demands of digitalization has exposed how essential renewable energy is to the future of our society. Modern culture demands batteries with sufficient capacity requirements for portable electronics with high cyclability and with power delivery sufficient for electric vehicles that reach hundreds of miles in range per charge. Since their commercialization by Sony in 1991, lithium-ion batteries have been the front line contenders of renewable energy storage for today's power applications. In this chapter, we will examine the components of a traditional lithium-ion battery along with their limitations and introduce an alternate solution in lithium-sulfur batteries.

## 1.1 Traditional Lithium-Ion Batteries

The chemical mechanism of a typical lithium-ion battery relies on the technique of intercalation, which is strongly dependent on the electrode's physical structure. Cathode and anode materials in traditional cells are designed so that they can house the volume of lithium ions with little to no change in their physical structure. Parallel oxidation and reduction reactions are the driving chemical forces behind the mechanism of lithium-ion batteries. A common lithium-ion cell has one electrode composed of lithium metal oxide while the opposite electrode is graphite.

Charging the cell results in the lithium containing electrode undergoing oxidation and releasing lithium ions to travel through the electrolyte and find lodging in the layered structure of graphite. At the same time, electrons from oxidation travel through an external circuit to serve the load. During discharge, the lithium ions migrate back through the electrolyte to their original position as the cathodic ion in lithium metal oxide.

Lithium-ion batteries based on this technique have played a crucial role in enabling widespread portable electronics. Intercalation batteries, however, are quickly reaching their limits in specific capacity, with maximum values between $140 - 200\,mA\,h\,g^{-1}$, and energy densities within $500-600\,W\,h\,kg^{-1}$. [2] The limits of energy density are not enough to support storage on MWh or GWh scale and as a result, new electrochemical mechanisms are being researched to gratify current demands.

## 1.2 Lithium Metal Anode

A practical idea to overcome the limits of traditional lithium-ion batteries is to utilize the maximum capability of lithium. Lithium the most electronegative metal on the periodic table. Due its extreme electronegativity (-3.04V vs. standard hydrogen electrode), lithium metal offers a high potential difference and in turn, specific capacity, reaching heights of $3860\,mA\,h\,g^{-1}$. The promise of a large potential difference declares lithium an anode material and the primary ion donor in an electrochemical cell. Researchers often use lithium metal as the negative electrode to test various cathode materials; a process called half cell testing.

There are two primary problems associated with lithium metal as the anode. The first is the build up of fractal deposits including needle-like, snowflake-like, tree-like, bush-like, moss-like and whisker-like structure referred to as dendrites upon charging/discharging the battery over many cycles. [3] Dendrites are a safety hazard in an electrochemical cell because, their build up can reach past the separator, to the cathode, and lead to an internal short circuit. A second major hurtle with lithium

anodes is that lithium ions reacts instantly with most organic electrolytes to form a solid electrolyte interphase (SEI) on the lithium metal. This SEI layer is ionically conductive but electrically insulating, suggesting that theoretically the SEI layer can aid in the mobility of lithium ions while limiting lithium metal's reactivity. Alas, while undergoing cycling the SEI layer becomes susceptible to mechanical failure and the lithium reactivity suppression is negligible. This often results in lithium metal anode's having cycling problems and poor Coloumbic efficiency retention. [4] Previous reports have determined the solution to passivate lithium and to create a stable SEI layer, is to add lithium salts to the electrolyte solution. Lithium salts tend to aid in the reduction process while protecting the SEI layer from failure. [5], [6], [7] However, the introduction of additional salt ions threatens an increase in parasitic reactions. Another tactic often used is to add excess electrolyte to the cell to boost the Coloumbic efficiency which reduces energy density. Although, batteries with lithium metal electrodes often have cycling problems, they still yield the best results when researchers are investigating cathode materials with high capacity. Currently, two major types of cathode materials are being tested with a lithium anode, namely, gaseous oxygen batteries and solid state sulfur batteries, with theoretical capacities reaching $1,200$ and $1,675\, mA\, h\, g^{-1}$, respectively. [8] This work reaches for high capacity and high energy density batteries by examining sulfur cathode materials.

### 1.3 Lithium-Sulfur Batteries

Lithium-sulfur batteries are an exceptional candidate to bring next level lithium based batteries to the horizon. A lithium-sulfur cell has three main components: a lithium anode, a carefully selected electrolyte and a sulfur based cathode. Like carbon, sulfur trends towards catenation, its most stable allotrope at room temperature is in the form of an octagon shaped ring ($\alpha$-cyclo octasulfur). The mechanism of a lithium - sulfur battery is demonstrated in the following image.

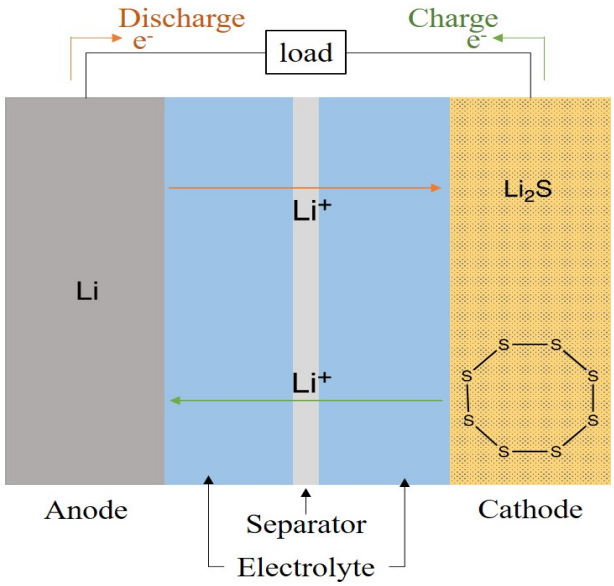


Fig. 1.1. Schematic of a Typical Lithium-Sulfur Battery

The lithium-sulfur cell's electrochemical mechanism begins with discharge. During discharge, oxidation occurs at the negative electrode, releasing lithium ions and electrons from the anode. The lithium ions move internally through the electrolyte while the electrons are transferred through an external circuit, producing electric current to feed the load. Sulfur is reduced on the cathodic electrode by accepting lithium ions to produce lithium sulfide, $Li_2S$. [9] The overall redox reaction is:

$$2Li + S \rightarrow Li_2S$$

Due to it's two unpaired valence electrons, sulfur accepts twice the number of lithium ions compared to transition metals, which can accept only a fraction of charge. Upon reduction, solid $\alpha$-sulfur is dissolved and disassembled according to the sequence, $S_8 \rightarrow S_8^{2-} \rightarrow S_6^{2-} \rightarrow S_4^{2-} \rightarrow S_2^{2-} \rightarrow S^{2-}$ which generates a series of intermediate lithium polysulfides $Li_2S_x$ $(2 \leq x \leq 8)$. [10] Eight sulfur atoms correspond to the equivalent of 16 lithium ions and electrons transferred in the reaction, which is the exact reason for such a high calculation of capacity. The advantage of a

lithium-sulfur cell is the high practical energy density, calculated from the capacity of the total lithium-sulfur cell and the average nominal voltage of 2.1 V. The exact calculations of theoretical capacity in a sulfur cathode is $1,675\,mA\,h\,g^{-1}$ and the expected specific energy delivered by a lithium based sulfur battery is $2,600\,W\,h\,kg^{-1}$. It seems that elemental sulfur is an incomparable candidate as a cathode material; however, it becomes apparent that the intermediate polysulfide species formed in the reduction process causes side reactions with the electrolyte and lithium anode while causing physical deformation to the cathode side of the cell.

### 1.3.1 Electrolyte Material

As the reduction of sulfur proceeds, higher order lithium polysulfides ($Li_2S_6$ and $Li_2S_8$) are formed, which cannot be fully reduced in common electrolytes; such as esters, carbonates or phosphates. Instead, suitable electrolyte choices for lithium-sulfur batteries are limited to the linear or cyclic ethers, such as 1,2-dimethoxyethane (DME) and 1,3-dioxolane (DOL), respectively. The inclusion of DME offers the benefits of high polysulfide solubility and quicker kinetic reactions but DME does not inhibit reactions with the lithium metal. On the other hand, DOL experiences low solubility and reacts slowly. There is a huge benefit that the SEI layer is significantly more stable when DOL is in the mix. [11] The solution is combination of DME and DOL that can sufficiently reduce the sulfur species and also protect the anode from degradation. The intermediate polysulfides causes troublesome reactions in the cell but without their formation, the reduction of sulfur exists only in solid phase ($Li_2S$, $Li_2S_2$, and $Li_2S_4$,) so the reaction can only occur on the cathode/electrolyte interface which means the depth of active material is not completely utilized and violent surface reactions lead to physical deformation of the electrode. Lithium salt additives are included in the electrolyte to passivate the lithium metal and impart stability to the SEI layer. Conventional lithium salts such as $LiPF_6$,$LiBF_4$, lithium bisoxalatoborate ($LiBOB$) and lithium diflouro(oxalo)borate ($LiBF_2C_2O_4$) are not reasonable

because of parasitic side reactions. In addition, these salts cannot be used in solution with DOL's cyclic structure as they will encourage the ring opening and additional chain reactions. [12] Bis(triflouromethane) sulfonimide (LiTFSI) and $LiNO_3$ lithium salts are of interest because of their low reported rate of lithium metal degradation, thermal and hydrolytic stability. [13] The most effective electrolyte of lithium-sulfur cells is a combination solvent of DME/DOL/LiTFSI with $LiNO_3$ additives.

The cycling performance of a lithium-sulfur cell is highly dependent on the concentration of polysulfides in the cell. An excess of polysulfides leads to the increased production of lower order solid lithium polysulfides that become inactive and deposit out of the electrolyte or become embedded in the structure of the separator. The ratio of electrolyte to sulfur (E/S) is used to measure the impact of polysulfide concentration. It is common to add an excess of electrolyte to achieve high cell performance over long term cycling, however, excess electrolyte can lead to the depletion of active material, which reduces the overall energy density of the cell. Finding the optimal balance of electrolyte to active sulfur material is a step towards batteries with high energy density and long cycle life. The optimal E/S value has been determined by reducing E/S ratios until a voltage delay appears at first discharge. This scrutiny concluded that for a lithium-sulfur battery to successfully surpass 100 efficient cycles, the E/S ratio must be $\geq 10\,\mu L\,mg^{-1}$. [14]

### 1.3.2 Cathode Material

Elemental sulfur and its constituent polysulfides are fundamentally insulating materials so a conductive material has to be added to complete the cathode. The common method to induced conductivity is to add a carbon containing substance along with the sulfur cathode. During reduction, the sulfur species undergoes a detrimental increase in volume of approximately $\sim$80%. [12] which means that the carbon matrix has to withstand a large mechanical shock. Therefore, the conductive carbon matrix must be sufficiently porous, leading to a decreased energy density. The primary cause

for failure in a lithium-sulfur cell is contributed to the shuttling mechanism, where the insoluble lithium polysulfides escape from the cathode and are lost in the electrolyte. The addition of a binder reduces the polysulfide side reactions and improves the cyclability of the cell. A binders main purpose is to facilitate lithium ion transfer while restricting the poylsulfide escape by anion metatheis. [15] Research efforts focus on optimizing the crystalline structure of carbon materials by tuning pore size to easily fit the discharge products. [16]

### 1.3.3 Anode Material

The lithium-sulfur batteries discussed in this document, use lithium metal as the anode material to maximize energy density and to test pioneering cathode materials. A stable SEI layer is chemically formed to limit the reactivity of lithium metal and prevent mechanical strain on the material. Dendrite formation in lithium-sulfur cells is less severe than lithium ion batteries because of the internal polysulides which react to reduce surface growth on the lithium anode. Although, the the polysulfide impart some stability to the anode, their reactions with lithium are the ultimate reason for unmatched theoretical capacity of sulfur cathodes.

## 1.4 Project Overview

Novel organosulfur materials are synthesized in this report, which solve three of the major problems with lithium-sulfur batteries. The troublesome higher order polysulfides are completely omitted in the design of this material. The series of materials engineered in this study minimizes the shuttle mechanism and as a result, the active material loss. The best ratio of electrolyte to active material will be analyzed to achieve the batteries performance under high loading conditions. Finally, the measured volume change of the novel cathode material is massively reduced compared to the traditional sulfur cathode. The material introduced in the future chapters reveals options to achieve high energy density lithium-sulfur batteries.

# 2. METHODS OF MATERIAL CHARACTERIZATION

The material proposed and developed in this report undergoes series of material characterization tests to prove the chemical composition and gather information about the material's physical structure. A description of the analytical techniques used throughout this research is summarized in this chapter.

## 2.1 Fourier Transform Infrared (FTIR) Spectroscopy

Infrared spectroscopy is a method to characterize the unknown material based on it's particular absorption spectra, essentially the molecular fingerprint of the substance. In IR spectroscopy, a source of light is directed to a beam splitter which distributes the wavelengths in two directions. Some of the beam travels to a stationary mirror while the rest hits a mirror that is moving. The separate beams recombine with constructive and destructive interference to form an inferogram, which is specific to an associated wavelength. The inferogram travels through the sample and a detector confirms whether the light passed directly through or absorbed any of the wave. The log of the intensity ratio comparing the background spectrum to the sample spectrum builds a profile over time. The dependent variable used in this technique is called the wavenumber, and it is a measure of the number of cycles a wave undergoes per unit length, in units of $cm^{-1}$. The detector uses the mathematical concept of Fourier transformation to convert the discrete set of data into a frequency representation. When combined, Fourier transformation and infrared spectroscopy provide information on the chemical composition of a sample due to the specific absorption ranges distinct to elements and molecular compositions. [17]

## 2.2 Ultraviolet Visible (UV-Vis) Spectroscopy

Ultraviolet visible spectroscopy is a technique which analyzes the absorption and reflection in the ultraviolet and visible range of wavelengths. A beam of light enters a monochrometer, which uses a prism to disperse the light across all wavelengths. Next, a beam splitter divides the light in two and directs one stream towards the unknown sample and the other through a reference cell. The beams exit the cells and enter individual detectors. The wavelength absorbance is dependent on the ratio of the of the intensity from the sample cell to the that leaving the reference cell. The absorbance trend with respect to the wavelengths in the UV-Visible range of light shows clear peaks where the maximum wavelength is observed, revealing information of the materials color. [18]

## 2.3 Electron Impact-Mass Spectrometry (EI-MS)

The technique of mass spectrometry is used to determine the mass of a unknown molecule. It does this in a three step process. Step one, is the ionization of the molecule. The most widely used form of ionization is known as electron impact. In electron impact ionization, gaseous phase molecules pass through a volume of induced potential difference where an electron beam is flowing perpendicular to the molecule's path. Electrons bombard the molecule and knocks an electron from the molecule's shell. The initial single positively charged molecule is called the parent ion. There are many of these collisions occurring in the sample, creating daughter fragments and radical species. The second step is mass filtration, where the ions formed are focused into a beam. When a magnetic force is applied perpendicular to the ions beam it causes the ions to experience a change in acceleration that is proportional to the ions mass. The final step is detection, which is accomplished by varying the magnitude of the force to tune and sort the detection by acceleration and the corresponding size of the fragment. The results are then summarized by the ions intensity with respect to

the mass over charge ratio (m/z). Most often the charge is approximately 1 and the ratio, m/z, accurately reflects the mass of the ion fragments.

## 2.4 X-ray Photoelectron Spectroscopy (XPS)

X-ray photoelectron spectroscopy is the study of the energy distribution of a material irradiated by x-rays. The photoelectric interaction between the x-ray and the sample causes the electrons to be emitted at discrete kinetic energies. The kinetic energy of the electron is related to the binding energy by methods of conservation. Quantitatively binding energy is unique to respective molecules and can therefore aid in material characterization. [19]

## 2.5 Scanning Electron Microscopy (SEM) and Energy Dispersed X-ray (EDX)

The process of scanning electron microscopy starts with a beam of targeted electrons pouring onto the surface of a unknown sample. The electrons from the beam can be absorbed, reflected or can induce the release of secondary electrons. The behavior that the surface exhibits when hit with electrons is detected and compiled to construct a high definition image of the sample's surface morphology. The resulting image displays detailed surface architecture at spacial resolutions ranging from 5-100 nm. In combination with SEM, Energy dispersive X-ray (EDX) spectroscopy measures excitation energy of the atoms on the surface. Detectors that measure low energy x-rays are located close to the materials while the surface is exposed to the SEM's electron beam. The emitted electromagnetic radiation represent the energy difference between two shells of an atom, sufficiently measuring the elemental composition of the surface. [20]

## 2.6 X-ray Diffraction (XRD)

X-ray diffraction utilizes the quantum nature of x-rays to obtain structural information about crystalline materials. An incident beam of x-rays targets the material and reflective wavelengths are scattered from the surface. In crystalline structures, the reflected x-rays diffract while experiencing constructive or destructive interference. The x-ray diffraction obeys Bragg's Law $n\lambda = 2dsin(\theta)$ where $\theta$ indicates the diffraction angle. Multiple scans across the surface of the sample form a diffraction pattern that is unique for reported molecular materials. [21]

## 2.7 Nuclear Magnetic Resonance (NMR) Spectroscopy

Nuclear magnetic resonance spectroscopy is used to confirm the purity of a sample and gives insight to its molecular structure. In a nutshell, NMR is a spectroscopic technique based on the absorption of electromagnetic radiation. Although there are many methods of NMR, $^1H$ is used in this study. The end goal is to use the unique qualities about the spin of hydrogen to identify the number of hydrogen atoms and their orientations. The spin of a hydrogen nucleus in the presence of a magnetic field has two options, spin up (1/2) or spin down (-1/2). Initially, a sample is placed in the NMR, and the nuclear spins are relaxed and randomly oriented. When an external magnetic field is applied, the nuclei snap into one of two possible states, either aligned with the magnetic field or directly opposed. This behavior is associated with the absorbance of hydrogen's resonance frequency, propelling it to a high energy level. When the nucleus' energy state returns to ground level a corresponding frequency is emitted. The received frequency and the intensity of that signal is used to develop an NMR spectra. A typical NMR spectra uses a chemical shift mechanism in ppm to display finding in a clear manner. Chemical shifting compares the difference of emitted frequency and a reference frequency induced by the magnetic field. The spectra obtained from NMR measures signal intensity in terms of the chemical shift. [22]

# 3. PHENYL POLYSULFIDE LIQUID CATHODE

## 3.1 Introduction

The significant volume changes that accompany the reduction of elemental sulfur to lithium sulfide has initiated the grand challenge of building a sufficient conductive matrix for the cathode to accommodate size variation. A satisfactory material must have high porosity to ensure intimate connection between the conductive matrix and the insulating active material. Research efforts have been dedicated to engineering the physical carbon containing material to adapt to the chemical changes of sulfur. Innovation in carbon material for a sulfur cathode is demonstrated in microporous, mesoporous or a hybrid structure to strongly adsorb the sulfur and expand in the presence of volume change. In addition, these micro/meso porous structures also contain the exasperating polysulfides and hinder their release into the electrolyte. Other cathode developments involve using carbon based materials, such as carbon black, hollow carbon spheres and carbon nanotubes (CNT), to impart a conductive matrix; these materials do not function as a container for the polysulfides. [23]

In this work, a series of organic phenyl polysulfides are fabricated; phenyl tetrasulfide (PTS), phenyl pentasulfide (PPS) and phenyl hexasulfide (PHS). The chemical structure of these compounds are linear sulfur chain bound with two phenyl groups at each end. The sulfur chain is engineered to eliminate the formation of high order soluble polysulfide anions. The liquid phase of these organic polysulfides foster an easy method of depositing active material on conductive CNT framework. The limited number of sulfur atoms in the chain greatly reduces the volume expansion common to lithium-sulfur batteries. Finally, in an attempt to achieve the highest possible energy density, this class of materials was tested with a high loading of active material attributed to a low electrolyte to sulfur ratio.

## 3.2 Experimental

### 3.2.1 Synthesis

Previously reported methods of bis(aryl) polysulfide synthesis require a parent thiol reacting with the appropriate order of sulfur chloride along with the aid of a pyridine catalyst combined in an anhydrous solvent [24] or require a base catalyzed reaction of thiols with elemental sulfur. [25] In this work, a method of fabricating phenyl polysulfides without the aid of a solvent or catalyst was employed for a one-step route to the product. Beginning with liquid benzethiol (PhSH), appropriate stoichiometric ratios of solid sulfur were added and mixed at 40° C. The physical structure of benzenethiol incorporates an the aromatic hydrocarbon ring. Figure 3.1a displays the chemical states and physical structures of the molecules involved in the reaction. The high acidity of the thiol group on aromatic benzenethiol causes the bonding of sulfur atoms, resulting in the formation of phenyl polysulfide. Sulfur acts as a nucleophilic species and donates an electron pair to the thiol group's proton, causing the condensation and emission of $H_2S$ gas. The rightmost image in Figure 3.1a provides evidence of $H_2S$ gas formation by the darkening of a lead acetate indicator.

Following the coefficient trend of the balanced chemical equation a $S_8$:PhSH ratio of 3:2 produces PTS, 4:2 yields PPS and 5:2 results in PHS. Physically, the gaseous emission of $H_2S$ was observed by the presence of bubbles during the reaction. To accelerate the redox reaction, the sulfur/benzenethiol mixture was heated to $40°C$ until completion. The mixtures volatile bubbling greatly subsided after 5 hours and ceased at the 6hr mark, signaling the end of the reaction. As expected, the density of the materials increases linearly with the order of sulfur atoms in the chain (Figure 3.1b). This facilitates an increasing trend in the gravimetric specific capacity (Figure 3.1c) and volumetric energy density (Figure 3.1d) along with polysulfide order.

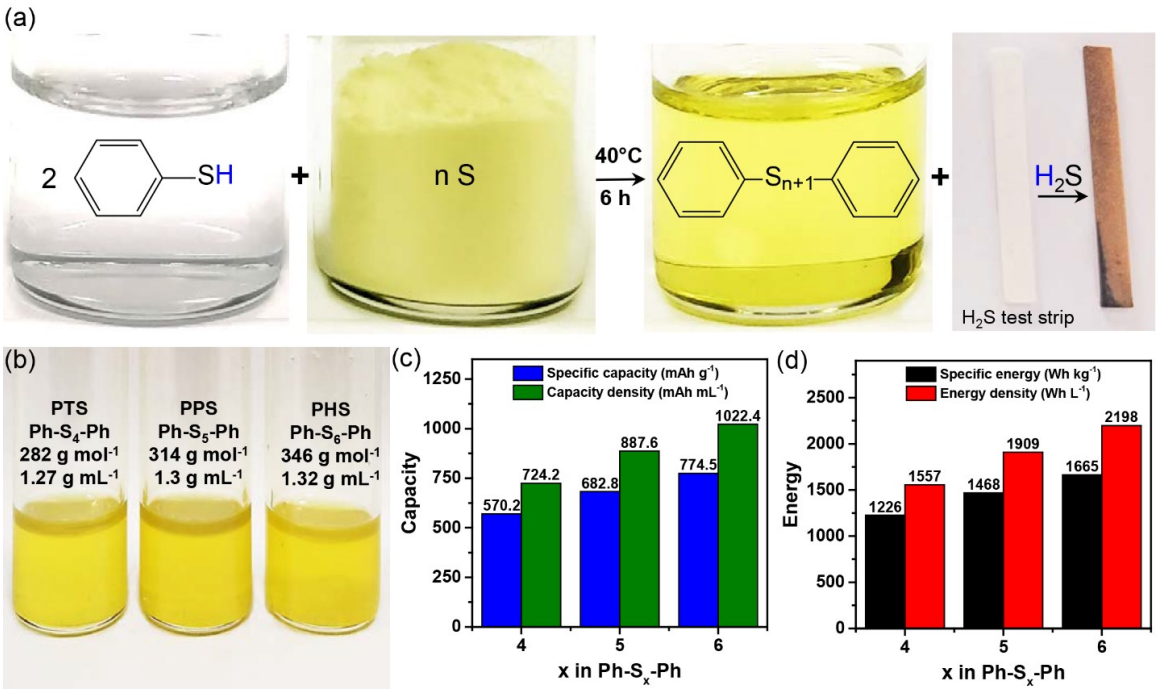


Fig. 3.1. (a) Equation along a visual representation of the phenyl polysulfide synthesis process. Lead acetate based test strip were used to confirm the $H_2S$ evolution. (b) Optical image of the liquid polysulfides along with their properties. (c) Theoretical specific capacities ($mAh\,g^{-1}$) and capacity densities ($mAh\,mL^{-1}$) of the different polysulfides and their (d) theoretical specific energies ($Wh\,kg^{-1}$) and energy densities ($Wh\,L^{-1}$).

### 3.2.2 Cell Assembly

One objective of this work is to address the problem of electrolyte to sulfur loading. Thus, two cell configurations have been developed and are reported here. The polysulfide batteries were built in a typical coin cell enclosure of the type CR2032. Binder free multi-walled carbon nanotube (CNT) paper, known commercially as buckeypaper, was used as the current collector. Subsequently, lithium metal was used as the anode. The electrolyte used is composed of $1.0MLiTFSI$ and $0.2MLiNO_3$ in a mixture with a solvent of DME/DOL (1:1 v/v), a Celgard 2400 separator was placed to restrict contact between the electrodes, nickel foam tops off the lithium anode to

reduce any empty space in the cell and enhance contact between the components. A second cathode was fabricated to test high active material loading. The high loading cathode was consisted of the same elements with ratios that resulted in an electrolyte/active material of $3\mu L\, mg^{-1}$.

### 3.3 Characterization

Prior to the synthesis of these three polysulfides, a series of spectroscopic tests were performed to confirm that the expected reaction was successful. FTIR spectroscopy was used to confirm the thiol group had been successfully depronated and replaced with a sulfur chain (Figure 3.2a). The S-H absorption peak is known to be approximately located at $2567\, cm^{-1}$. [26] The S-H peak is clear in the spectrum corresponding to PhSH but it is not present in the spectra for PTS, PPS and PHS. The information gathered from FTIR evidence confirms the conversion of thiols to a polysulfide chain.

UV-Vis spectroscopy was used to validate the increasing number of sulfur atoms. The results of UV-Vis spectroscopy are shown in Figure 3.2b which includes phenyl disulfide for comparison to the collected PTS, PPS and PHS spectra. The peak absorbance for all four species lies in the wavelength range between 380 and 405nm; the absorption range of the series corresponds to the transmittance wavelengths in the range $570 - 575\, nm$, also known as, yellow. The sulfur concentration and associated yellow color should increase along with the number of sulfur atoms. The increase in sulfur concentration is demonstrated by the increasing peak wavelength across the polysulfides order. In order to graphically demonstrate the linear order, peak wavelength was plotted versus the square root of the number of sulfur atoms. The inset image in Figure 3.2b demonstrates the visible linear trend.

Confirmation of the purity of the fabricated polysulfides was obtained by EI-MS. The mass spectra of PTS (displayed in Figure 3.2c) exhibit a peak at m/z of 281.96 agreeing with the molar mass. Molecules and radicals containing thiols, sulfur chains

and phenyl rings are also revealed in mass spectroscopy, however, the absence of peaks beyond the 280 range indicates there are daughter fragments of PTS and confirms the purity. Similarly, the spectra for PPS, displayed in Figure 3.2d reveals a maximum m/z values of 313.98 corresponding to the expected molecular mass. EI-MS of PHS exhibits an associated m/z value of 345.92 along with daughter fragments including the lower order polysulfides, PTS and PPS.

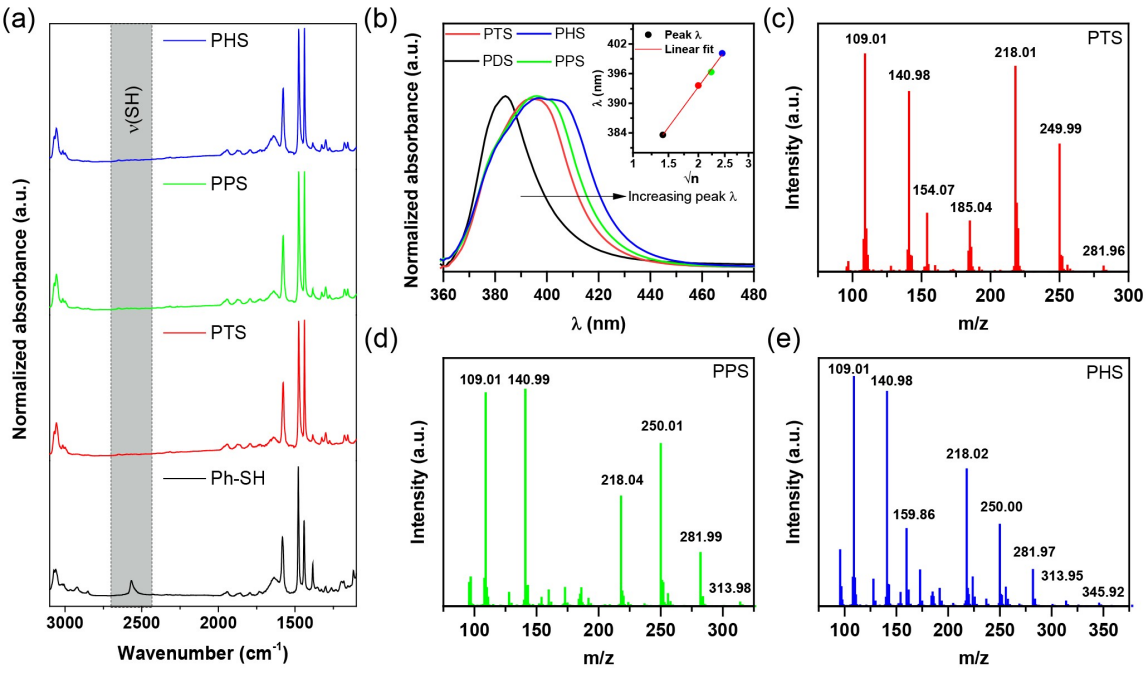


Fig. 3.2. (a) FTIR spectrum of benzenethiol (Ph-SH) and the synthesized phenyl polysulfides. (b) UV-Vis spectra of equimolar solutions of different phenyl polysulfides along with that of phenyl disulfide (PDS) as reference. Inset of (b) shows the linear increase in peak  as a function of number of sulfur atoms. EI-MS spectrum of (c) phenyl tetrasulfide (PTS), (d) phenyl pentasulfide (PTS), and (e) phenyl hexasulfide (PHS).

## 3.4 Results and Discussion

PTS, PPS, and PHS were developed using a simple one-pot method of synthesis, the products have been confirmed using a series of spectroscopic characterization

methods. The next step is to evaluate the behavior and ability of the cathode materials under electrochemical testing. Coin cell batteries were examined via cyclic voltrammetry (CV) at a rate of 1C to expose nuances in the chemical mechanism. In CV, the voltage of the working electrode is measured against a reference electrode. This technique in commonly employed in battery technology to investigate the reduction and oxidation process. In this report we use CV to gather insight into the dissolution/recombination steps during the redox reaction.

The CV results for the three materials are displayed in Figure 3.3a. In the cathodic scan for all materials there are three distinct reduction peaks. At the 2.4 V mark, the polysulfides experience the breakage of the S-S bonds in their respective structures. Previous reports have demonstrated that as the order of S-S bonds increases, the bond energy is lowered. [27] Thus, the variations in bond energies are reflected in the staggered reduction currents. At 2.2 V, the reduction of the lithium polysulides is facilitated by the formation of a phenyl persulfide and phenyl sulfide radical. [28] The final reduction peak at 2 V corresponds to the complete conversion of low order lithium polysulides ($Li_2S_x$, $2 \leq x \leq 4$) to lithium sulfide ($Li_2S$) and the formation of lithium thiophenolate (PhSLi). [29] The anodic scan reveals two major oxidation peaks. The majority of the restoration of phenyl polysulfides occurs at 2.3 V and full conversion at 2.4 V.

Galvanostatic cycling was used to evaluate the performance of the cells under long term cycling. Operating at a C/2 rate, Figure 3.3b demonstrates the resulting voltage profiles of PTS, PPS and PHS. PPS and PHS exhibit a slight discharge plateau at 2.35 V while PTS shows a sloped region until 2.25 V. A second discharge plateau is observed at 2.15 V for PTS and 2.2 V for PPS and PHS. The final plateau at 2 V confirms the complete reduction to lithium polysulfide. The voltage plateaus along the reduction path correspond to the same chemical finding of CV. The ability of sulfur to boost capacity is demonstrated in the trend of increasing specific capacity along with order.

Physical and chemical changes in the cathode were traced using appropriate microscopy and spectroscopy techniques. To confirm the proposed mechanism, a discharged cathode was probed with XPS (Figure 3.3c). XPS revealed broad peaks located at 161.6 eV, characteristic of PhSLi and 160.2 eV, confirming $Li_2S$ as a discharge product. XPS confirmed the discharge products were as theoretically expected. SEM was utilized to provide insight on the morphological changes occurring at discharge. The SEM image for PHS is displayed in Figure 3.3d and represents the characteristics of the discharged cathodes of PPS and PTS. The SEM image shows all the discharged products coating the CNT core. The products completely cover the carbon structure, suggesting parasitic side reactions due to shuttling, are at low risk. The uniform distribution of discharge product is also a good indicator of consistent electrical contact between the active material and conductive matrix. EDX confirms the distribution of sulfur and carbon on the electrode's surface.

The phenyl polysulfides were tested at a 1C rate to exemplify the long term cycling of these materials (Figure 3.3e). Results show PTS delivers $514\,mA\,h\,g^{1}$ which suggests a 90% material utilization. PTS is able to maintain a capacity of 65% over the duration of 300 cycles. PPS successfully delivers a capacity of $612\,mA\,h\,g^{-1}$ at a rate of 89.6% material utilization and continues to retain a capacity of 75% over 300 cycles. Finally, the PHS proved $650\,mA\,h\,g^{-1}$, a utilization of 84%. PHS was by far the most stable electrode, with the ability to reach 800 cycles without falling below a capacity retention rate of 80%. All the reported rates are at least two times the current capacity of traditional lithium-ion batteries, signifying their substantial benefits to battery research. The exceptional ability of the PHS material provides promise in the progression of lithium-sulfur batteries.

Consumers of modern portable electronics demand the option of fast charging. Thus, the PHS cell was tested at a number of C-rates including C/2, 1C, 2C, 3C, 4C, 5C and 10C over 10 full cycles.

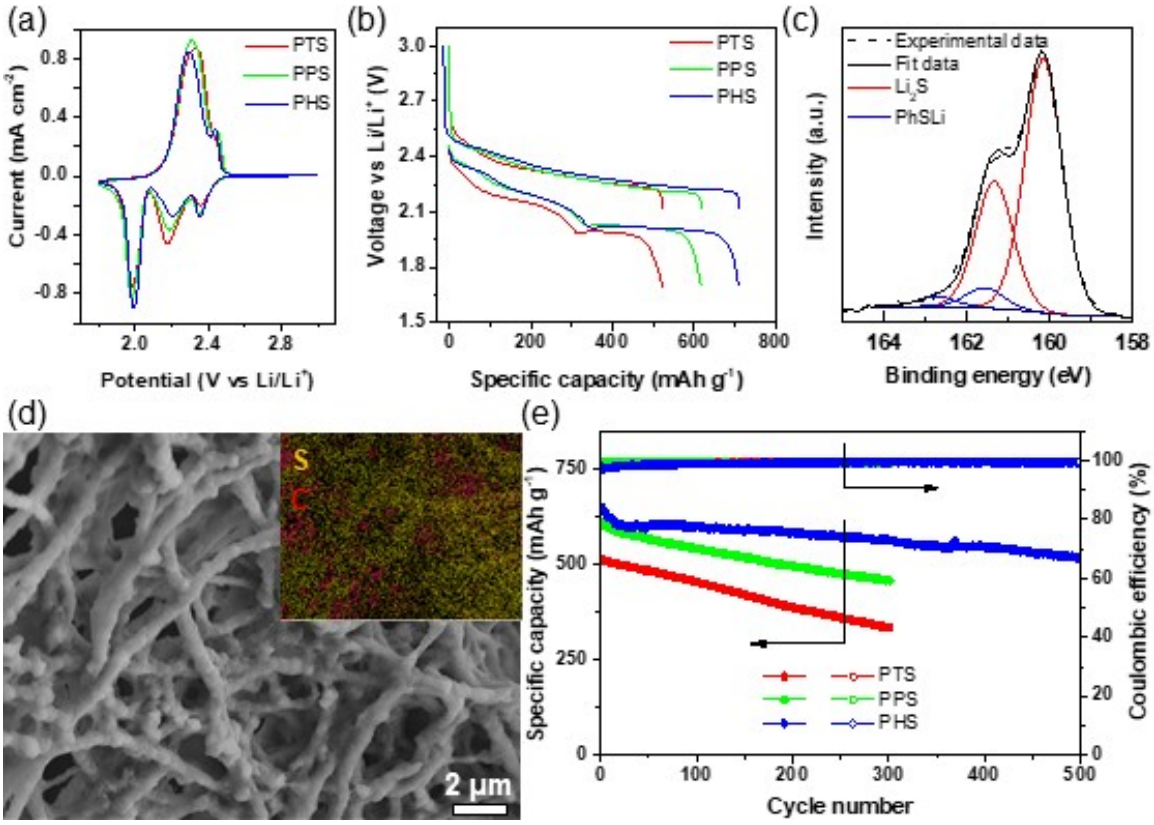


Fig. 3.3. (a) Cyclic voltammetry (CV) of the phenyl polysulfide cathodes. (b) Voltage profile of the polysulfide cathodes cycled at C/2. (c) Sulfur XPS spectrum of the PHS cathode in the discharged state. (d) SEM of the PHS cathode in the discharged state along with its inset EDX mapping and (e) long term cycling performance of the polysulfides at 1C.

Figure 3.4a demonstrates the ability of the batteries at accelerated charge rates. All of the tested rates demonstrate electrochemical stability over 10 cycles. Even at a high current rate, the PHS cathode exhibits a capacity greater than $400\,mA\,h\,g^{-1}$, corresponding to a material utilization of 50%.

One of the major hurtles of high energy density batteries, is the exorbitant electrolyte/active material required for scalability. A high PHS active material loaded cell was created with $E/S = 3\mu L\,mg^{-1}$. Figure 3.4b conveys the highly loaded PHS cathode can reach areal capacity heights of $7.6\,mA\,h\,cm^{-2}$, which is much higher than reported values of commercial lithium-ion batteries. [30] In addition, stable cycling is

achieved over 50 cycles with a capacity retention of 80% at such low electrolyte content. The observed fading is attributed to an aggressive electrolyte consumption. It is demonstrated that under high loading, PHS can offer an impressive specific energy of $1,302\,Wh\,kg^{-1}$ and energy density of $1,702\,W\,h\,L^{-1}$.

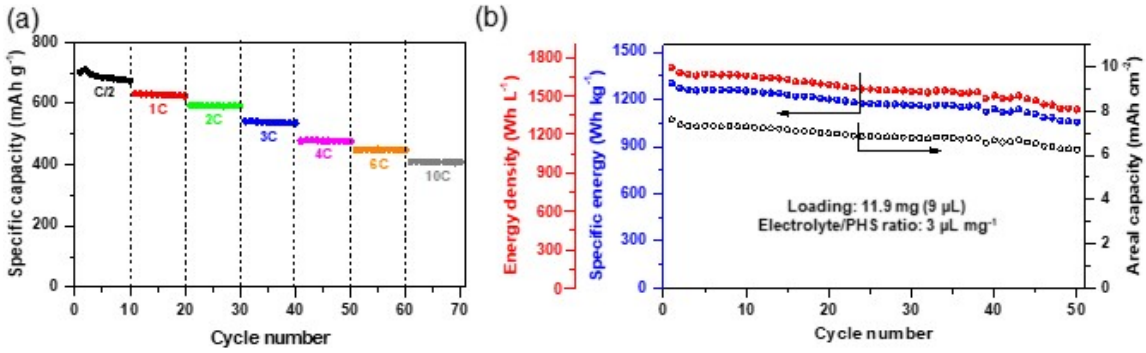


Fig. 3.4. (a) Rate performance of highly loaded PHS cell collected over 10 cycles at C rates ranging from C/2 to 10C. (b) Cycle performance of heavily loaded PHS cell with effective $E/S = 3\mu L\,mg^{-1}$

## 3.5 Conclusion

This cathode materials solves three major problems posed by traditional sulfur electrodes: Primarily, the dissolution of intermediate polysulfides is eliminated due to the limited number of sulfur atoms that exist in the organic molecule. Secondly, the novel material content results in a significantly reduced volume change upon discharge. The volume change of the respective cathode materials was calculated to be 36.9% in PTS, 37.32% in PPS and 37.08% in PHS, representing a practical electrode design. Finally, the active PHS electrode successfully cycled 50 times with a low $E/S$ ratio, demonstrating a significant increase in energy density. The results claim that an organosulfur containing cathode is an innovative approach to achieving lithium-sulfur batteries with good electrochemical performance and high energy density.

# 4. PHENYL TETRASULFIDE POLYMER CATHODE

## 4.1 Introduction

The portable electronics market is constantly experiencing new and innovative technologies, which continue to propel electronics into the future. Among many demands for modern electronics is the ability for electronics to stretch, bend and roll and is a challenge for material scientists. The emergence of flexible electronics requires the materialization of lithium batteries, which not only offer high energy density but also have components that can withstand repeated mechanical strains. Current efforts in flexible energy storage involve the use of flexible conducting polymers, such as polypyrrole (PPy), polyaniline (PANI) and polythiophene (PTP), [31] or paper based lithium batteries [32]; however, these batteries fail to match cycling ability and capacity requirements.

This project has confirmed that phenyl polysulfides are exceptional cathode candidates for high capacity lithium-sulfur-batteries. The technology created in the previous chapter can be taken to the next level, due to the many accounts of co-polymerization of thiol-ene groups with sulfur backbones [33], [34] In this work, a highly flexible polymer phenyl tetrasulfide (PPTS) has been created as an efficient cathode material. The fabricated polymer is a repeating unit of a phenyl ring with four sulfur atoms attached linearly. Due to the three S-S bonds in the polymers architecture, this material can accept 6 electrons leading to a high theoretical specific capacity of $788\,mA\,h\,g^{-1}$. The polymer developed in this study is a revolutionary material that has the potential to be a major contributor in the progress of flexible battery technology.

## 4.2 Experimental

### 4.2.1 Synthesis

The method to form a high sulfur content polymer is mediated by sulfur's inherent nature to polymerize, as well as, the acidity of thiol groups. Here we exploit the deprotonation of 1,4-benzenedithiol's characteristic thiol groups to incorporate a fourth order sulfur chain. The leftmost species of the reaction shown in Figure 4.1a, is the construction of 1,4-benzenedithiol as a benzene ring with two thiol groups directly opposed. The corresponding image in Figure 4.1a, shows the physical properties of 1,4-benzenedithiol, exposing its nature as a fine white powder. 1,4-benzendithiol and distinctive yellow sulfur powder were incorporated into a toluene and carbon disulfide solvent to form a product of liquid PPTS. Excess sulfur abets the reaction by seizing the removed protons and evolving hydrogen sulfide gas. Evidence of gas evolution was provided via the color change of lead acetate hydrogen sulfide gas test strips when exposed to the PTS solution.

The para aromatic structure of 1,4-benezenedithiol encourages the formation of long chain linked units, sufficient for polymerization. The oily polymer membrane was formed by heating the the polymer solution to $125°C$ in a Teflon vessel at a rate of $5°C$ per minute. The mixture was held at $125°C$ for 12 hours to completely remove the solvent and create a firm membrane. Figure 4.1b demonstrates the size, color, transparency, and flexibility of the manufactured polymer. Adding a comprehensive volume of liquid PPTS to commercial CNT (buckypaper) paper and drying the composite in a vacuum transforms the polymer into a working conductive electrode and imparts a supporting framework. Figure 4.1c displays the flexibility and size of the PPTS-CNT electrode.

SEM imaging was used to confirm the submersion of CNT in PPTS. Figure 4.1d displays the results of SEM, revealing a network of porous CNT paper with a blanket of PPTS interwoven in the depths of the material. SEM alone does not fully describe the sulfur dispersion throughout the CNT paper. In order to get an idea of the

amount of sulfur in the cathode, EDX elemental mapping was employed (Figure 4.1d inset). EDX reveals an even distribution of sulfur surrounding the carbon nanotubes, suggesting an even portioning of PPTS in the material.

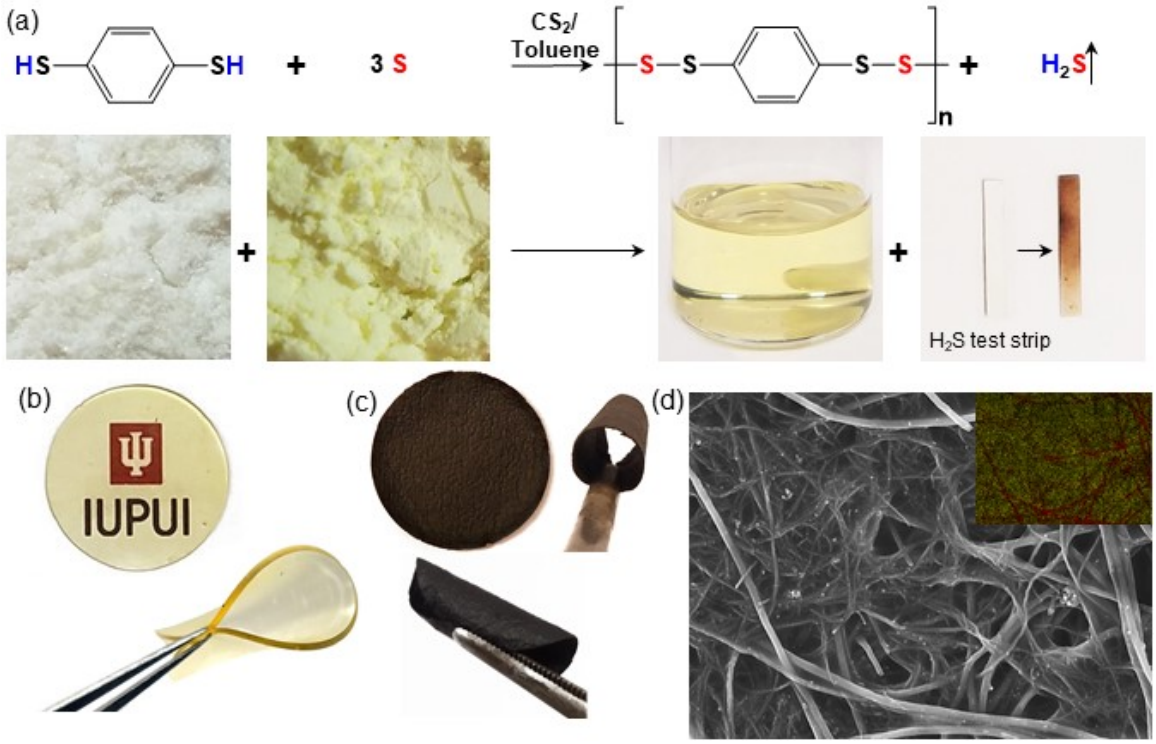


Fig. 4.1. (a) Equation and visible representation of the synthesis of polymer phenyl tetrasulfide. lead acetate based strips were used to confirm the evolution of $H_2S$ gas. (b) Optical image illustrating size, transparency and color of phenyl tetrasulfide polymer membrane. (c) Optical image representing the physical appearance of polymer phenyl tetrasulfide and carbon nanotube paper composite. (b) SEM image illustrating surface details of PPTS-CNT cathode along with its inset EDX mapping

### 4.2.2 Cell Assembly

The electrochemical performance of the fabricated PPTS-CNT composite was evaluated using standard coin cell. The electrolyte solution used in this process was 1.0 M of LiTFSI in 1,2-DME and DOL (1:1 v/v) with a 0.2 M $LiNO_3$ additive to

passivate the lithium metal anode. A Celgard 2400 separator was employed to isolate the electrodes. The lithium metal anode was topped off with nickel foam to fill the volume of the coin cell.

### 4.3 Characterization

One goal of this research effort was to develop a material that can be used in a flexible lithium battery. A flexible cathode component must have the ability to bend and stretch alongside the source electronic. A polymer material has been developed to serve as the cathode in a flexible battery. In order to confirm the nature a polymer several spectroscopic techniques were used for analysis. XRD analysis requires that a solid crystalline structure must exist for material identification. In the case of a polymer, an amorphous, noisy spectrum is expected. Figure 4.2a compares the XRD results of pure sulfur, 1,4-benzenedithiol, the PPTS membrane, and the PPTS-CNT cathode material. The XRD results reflect the characteristic *fddd* orthorhombic crystalline structure of elemental sulfur and demonstrates the characteristic peaks of 1,4-benzenedithiol's solid phase. The non-crystalline structure of the PPTS confirms it's amorphous molecular structure. The XRD analysis of the PPTS-CNT electrode provides a similar amorphous structure aside from a distinctive peak contributed to carbon 002. [35] This technique demonstrated the polymer nature of the PPTS and the composite PPTS-CNT.

FTIR is applied to the sample to attempt to prove that the reaction mechanism went as predicted. FTIR demonstrates the complete replacement of the thiol group attributed to the disappearing S-H absorption peak shown in Figure 4.2b. This evidence suggests the beginning of the expected reaction.

Further investigation into the mechanisms of the reaction can be accomplished with the help of NMR spectroscopy. The spectra in Figure 4.2c compares the NMR results of 1,4-benzenedithiol with that of PPTS. NMR reports the location and intensity of hydrogen atoms in the molecule. The notable difference between the spectra

is the minimal intensity of the thiol group's hydrogen in PPTS. This minimization suggests that the thiol's hydrogen was removed to incorporate sulfur atoms. A significant piece of evidence to support this theory is the intensity of the hydrogens in the benzene ring unchanged magnitude overall. NMR, FTIR and XRD corroborate the building blocks of PPTS.

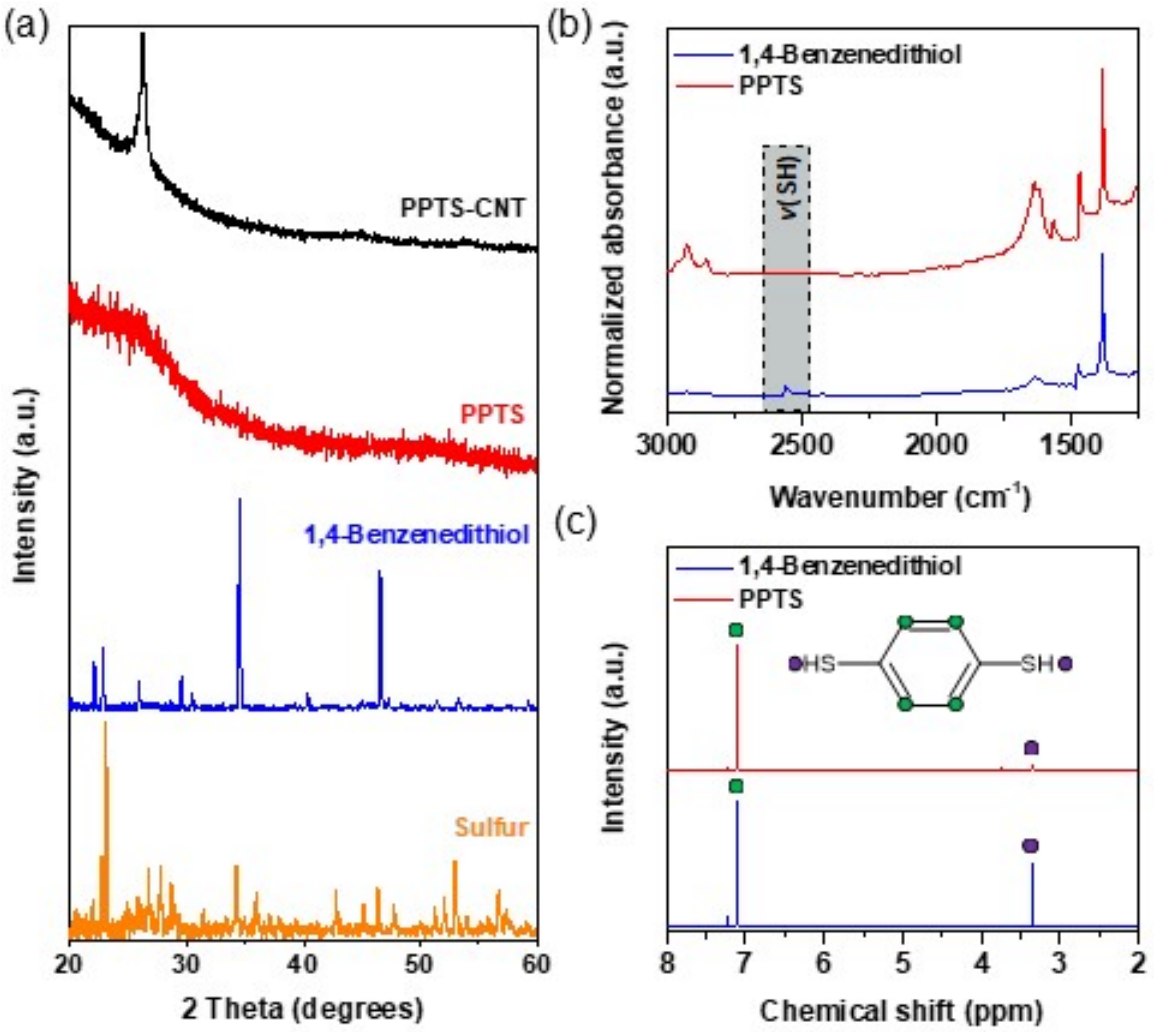


Fig. 4.2. (a) X-ray diffraction data symbolizing the polymer nature of PPTS. (b) SEM data signifying the elimination of thiol. (c) NMR data confirming the existence of an aromatic ring and thiol groups.

### 4.4 Results and Discussion

The coin cell assembly was subject to electrochemical testing via cyclic voltrammetry and galvanostatic testing. CV results are demonstrated in Figure 4.3a. Four reduction peaks are located at the 1.8 V, 2.1 V, 2.2 V and 2.3 V. The bond energy of a sulfur attached to a similar sulfur atom is found to be in the range 1.43-1.45 eV whereas, a sulfur atom bound directly to the phenyl ring has a bond energy calculated between 1.68 and 1.87 eV. [29] Due to the fact the S-S bond has less energy it is expected to be the first bond to break. The high voltage reduction peaks in the 2.2-2.3 V range correspond to the breakage of the polymer links according to the reaction $SSRSS + 2Li \rightarrow 2LiSSRSSLi$ where R stands in for the central phenyl group. The lower voltage plateau at 2.1 represents continuing reaction $2LiSSRSSLi + 2Li \rightarrow LiSRSLi + 2Li_2S_2$. The final reduction peak near 1.8 V is attributed to the dissolution of $Li_2S_2 + 2Li \rightarrow 2Li_2S$, recovering what is seen in a typical lithium-sulfur battery. The anodic scan reveals two oxidation peaks, corresponding to the formation of $Li_2S_2$ and the final reformation of the polymer.

Galvanostatic battery cycle reveals a voltage profile which can be used for further insight into the chemical mechanism. Figure 4.3b compares the voltage profiles for the charge/discharge of the cell at at slow C/20 rate and typical rate of 1C. The initial voltage plateaus at 2.4 V and 2.2 V, for the respective rates of C/20 and 1C, represent the first sulfur bonds breaking. The introduction of $Li_2S_2$ administers a voltage drop at 2.3 V for slow C/20 rate and 2.1V for 1C rate. The final voltage plateau is accredited to the final transition to $Li_2S$. At the slowed C-rate of C/20 a final capacity of $700\,mA\,h\,g^{-1}$, corresponding to a capacity increase of 12% with respect to $625\,mA\,h\,g^{-1}$ registered at a 1C rate.

The battery was subject to 350 cycles to predict it's capability over time. The results of electrochemical testing are demonstrated in Figure 4.3c. The initial discharge capacity is $625\,mA\,h\,g^{-1}$and after 350 cycles the discharge capacity sinks to $450\,mA\,h\,g^{-1}$, corresponding to a 72% retention in capacity. Capacity fading is likely

due to electrolyte decomposition within the cell and irreversible reactions of the phenyl ring. The Coloumbic efficiency maintains $\geq 99.5\%$, indicating ample cycle stability in the cell. The cell was subject to testing with quick C-rates over 10 cycles. C-rate analysis was noted at 1C, 2C, 3C, 4C and a recovery cycle at 1C (Figure 4.3d) and found to have initial capacities of 625, 550, 525 and 450 $mA\,h\,g^{-1}$, respectively, with the recovery cycle reaching $600\,mA\,h\,g^{-1}$. As each test continues there is a decreasing trend except for in the case of a 4C rate, which experiences and higher capacity after 10 cycles of $500\,mA\,h\,g^{-1}$. A key note is that one the cell recovered a capacity rate of $600\,mA\,h\,g^{-1}$, a retention rate of 96%.

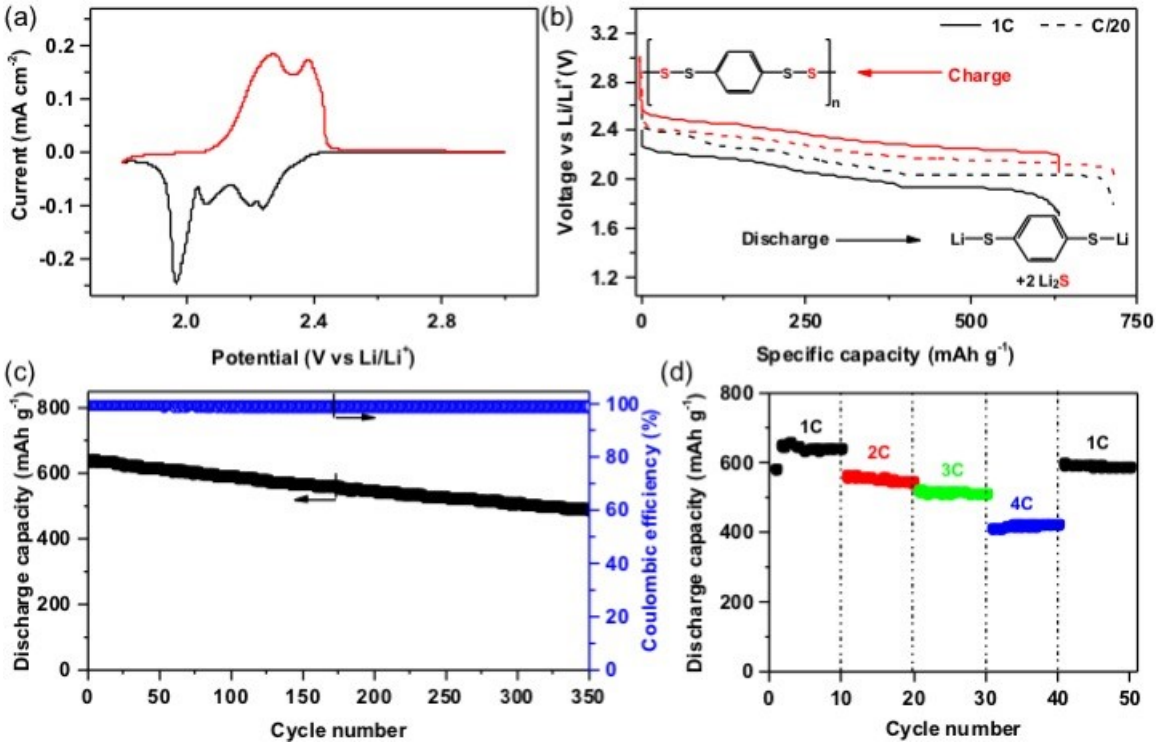


Fig. 4.3. (a) Cyclic voltammetry (CV) of the polymer phenyl tetrasulfide cathode. (b) Voltage profile of the tetrasulfide cathode cycled at C/20 and 1C. (c) Long term cycling performance of PPTS electrode at a 1C rate. (d) SEM of the PHS cathode in the discharged state along with its inset EDX mapping and (e) Cycling performance of PPTS cathode at rates ranging from 1C to 4C.

It has been demonstrated that PPTS is a quite capable cathode material. However, material testing is required for proof this cathode is fit for flexible application. In this work we have tested the material under tensile and bending strain to push its limits. Electrochemical cells are cycled after undergoing repetitive bending and stretching to get a picture of the longevity of the material. Figure 4.4a and 4.4b showcase the PPTS membrane and the PPTS-CNT composite under axial loading. The results report for PPTS there is a 334% increase in overall length while PPTS-CNT is able to lengthen 107%. For comparison, The tensile ability of CNT alone was also measured, demonstrating a mere 12% increase in length before cracking. Therefore, the addition of PPTS to a CNT network leverages a 89% increase in elasticity.

CV was used to analyze the reduction/oxidation details of the cathodes after undergoing mechanical strain. The voltage profile comparison of the cathode with no strain, 50 cycles of stretching and 50 cycles of bending is illustrated in Figure 4.4c. The three voltage plateaus correspond to the breaking of sulfur bonds, the formation of lithium polysulfides and the final formation of lithium sulfide.

Galvanostatic battery testing reveals the cyclability of the strained cells (Figure 4.4d). The initial discharge capacity of the cell with no strain, 50 cycles bent and 50 cycles stretched are 634, 600, 599 $mA\,h\,g^{-1}$, respectively. A lower discharge capacity is obvious for those materials undergoing strain. Cycling 200 times gives an overall idea of the capacity retention of these materials over time. Cathodes with no strain retain 86% of it's capacity. A cell that has undergone 50 cycles of bending maintains 79% of it's capability and the cathode material that experienced 50 cycles of stretching retained 86% of its initial capacity.

Analyzing the voltage profile and the galvanostatic testing profile in tandem questions the stability of the cathode with 50 cycles of bending. In the voltage profile, the plateaus are sloped and ill-defined, which is attributed to the stored strain energy in the $S-S$ bond. In the case of bending the slightly higher discharge/charge voltage is due to the application of both compressive and tensile stress in the bent motion. The galvanostatic testing demonstrates a high initial discharge capacity and

a retention rate of 79% throughout cycling. The comparable discharge capacities an high respective capacity retention are the reasons that this polymeric material is a good solution as a flexible batteries cathode.

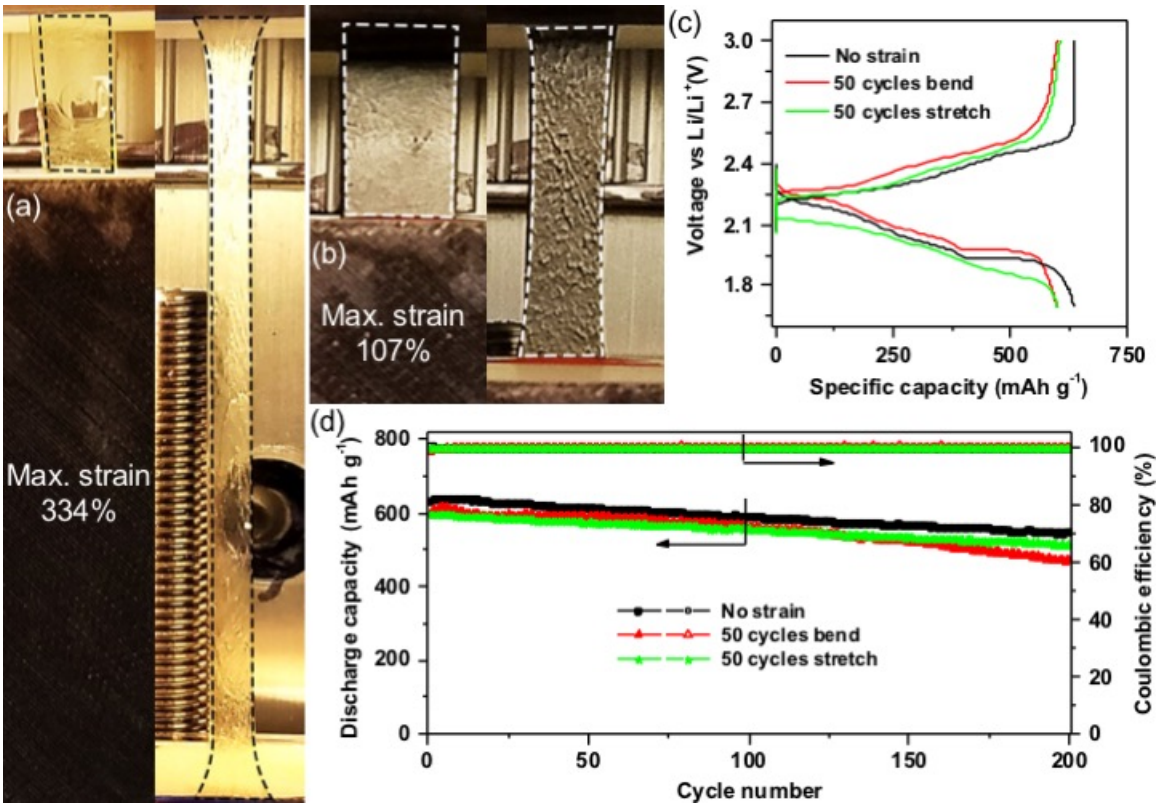


Fig. 4.4. (a) Tensile stretch of PPTS membrane. (b) Tensile test of PPTS-CNT composite electrode. (c) Voltage profile of the PPTS electrode's performance after 50 cycles of bending, 50 cycles of stretch stretching and no mechanical strain. (d) Long time cycling performance of electrode after mechanical stress.

## 4.5 Conclusion

Curved screens and bendable electronics are next level technologies of the future. The material developed in this chapter is a robust polymer which exhibits unmatched cycling performance before and after repeated mechanical strains. The novel chemical

technology of this material and the exciting ability to bend, makes it a potential solution to flexible lithium-sulfur batteries.

The phenyl tetrasulfide polymer reached the maximum capacity range of $633 - 700\,mA\,h\,g^{-1}$, generating an energy density between $1,266 - 1,400\,W\,h\,kg^{-1}$. Subsequent to strenuous stretching and bending of the electrode, it continued to reach capacity values of $600\,mA\,h\,g^{-1}$, which is three times what a typical lithium-ion battery can output. A polymer cathode material fabricated of phenyl tetrasulfide exemplifies a sustainable and satisfactory solution for energy storage in flexible electronics.

# 5. SUMMARY

There is no doubt that lithium-ion batteries have changed the cultural dependence of energy. The ability to store power for portable uses has opened the doors to an explosion of new technology. The need for reliable battery storage is always increasing and consumers are demanding higher cyclability, capacity and energy density. Traditional lithium-ion batteries are no longer able to keep up with energy storage use.

Portable electronics are continuously finding innovative ways to challenge researchers. Consumer ask for portable electronic batteries that hold ample charge over a long lifetime. In addition, innovative technologies are incorporating curved structures and materials, which causes a necessity of bendable and stretchable batteries. Modern electric vehicles require a power source not only has the necessary stability but can also deliver enough power for considerable range of motion per charge. Power generation from solar and wind is becoming increasingly more common and battery reservoirs on the GWh scale are crucial to long term stability.

Half cell testing of new cathode materials is amethod of research to investigate alternative battery materials that promise improved performance. This report analyzed the potential of a novel organic sulfur containing material that could accelerate the future of energy storage. The new sulfur containing material was developed to overcome many of the commonly seen challenges in typical lithium-sulfur cell. This material avoided the problematic side reactions that degrade the cell. Employing this material lead to a significant reduction in cathodic volume expansion. High active material loading of this cathode material demonstrates stable cycability and high performance of such cells. Finally, this material was developed with the ability to polymerize, which promotes the concept of flexible electronics in grasp. These new electrodes are an excellent contender as a component of next generation lithium batteries.

To overcome many of the challenges in lithium-sulfur batteries and new material was developed in the report that has the potential to lower the detrimental volume expansion, stability under high loading conditions and the additional benefit of flexibility. The capacity heights of this material reached $650 mAh\, g^{-1}$ in liquid organosulfur phenyl hexasulfide and maintained over $400 mAhg^{-1}$ at a high current rate. This material also demonstrated that it can withstand high active material loading and returned energy of the magnitude $1,302\, Wh\, kg^{-1}$. The volume expansion of elemental sulfur is reduced from 80% cathode expansion to 37%, suggesting the overall durability of cell. The polymerization of phenyl tetrasulfide (PTS) gives the material the benefit of imparted flexibility. Even under mechanical strain, the material reaches $600 mAhg^{-1}$, quadrupling the limits of current lithium-ion batteries. The novel cathode material developed in this study could be the missing piece to fabricating efficient and resilient lithium-sulfur batteries.

# 6. RECOMMENDATIONS

The phenyl polysulfides developed in this study demonstrate the plausibility of organosulfur containing cathode materials. Further engineering of the functional groups attached to the sulfur chain could present additional solutions to the problems posed by lithium-sulfur batteries.

More information about the polymer phenyl tetrasulfide will supply a better idea of the materials properties. Mechanical testing to reveal the materials Young's modulus and ductility could help determine it's best fit application. The electrical and thermal conductivity was be useful to know in order to solidify the materials limits. MALDI-TOF spectroscopy could be used to determine the number of repeating units that are in the polymer to get a grip on it's size.Classifying the polymer as a thermoset, theroplastic or elastomer would give some insight on its molecular composition.

Finally, although the use of renewable energy storage significantly decreases $CO_2$ emissions overall, the polymer developed in this research releases $H_2S$ gas. $H_2S$ gas is a very toxic material that has fatal effects thus, the practical implementation of these batteries material must include a way to harness the gas. A method known as the Claus process is a large scale operation to recover solid sulfur material from hydrogen sulfide gas. Further investigation into the Claus mechanism is beneficial to decrease the toxicity of synthesis and can possible be harness to return sulfur within the cell.

# REFERENCES

# REFERENCES


[1] N. Abas, A. Kalair, and N. Khan, "Review of fossil fuels and future energy technologies," *Futures*, vol. 69, pp. 31 – 49, 2015.

[2] H. Cheng and S. Wang, "Recent progress in polymer/sulphur composites as cathodes for rechargeable lithium-sulphur batteries," *Journal of Materials Chemistry A*, vol. 2, no. 34, pp. 13 783–13 794, 2014.

[3] W. Xu, J. Wang, F. Ding, X. Chen, E. Nasybulin, Y. Zhang, and J.-G. Zhang, "Lithium metal anodes for rechargeable batteries," *Energy & Environmental Science*, vol. 7, p. 513, 10 2013.

[4] N. Li, Y. Yin, J. Li, C. Zhang, and Y. Guo, "Passivation of lithium metal anode via hybrid ionic liquid electrolyte toward stable li plating/stripping," *Advanced Science*, vol. 4, no. 2, p. 1600400.

[5] V. Etacheri, R. Marom, R. Elazari, G. Salitra, and D. Aurbach, "Challenges in the development of advanced li-ion batteries: A review," *Energy & Environmental Science*, vol. 4, 01 2011.

[6] F. Ding, W. Xu, G. L. Graff, J. Zhang, M. L. Sushko, X. Chen, Y. Shao, M. H. Engelhard, Z. Nie, J. Xiao, X. Liu, P. V. Sushko, J. Liu, and J.-G. Zhang, "Dendrite-free lithium deposition via self-healing electrostatic shield mechanism," *Journal of the American Chemical Society*, vol. 135, no. 11, pp. 4450–4456, 2013.

[7] W. Li, H. Yao, K. Yan, G. Zheng, Z. Liang, Y.-M. Chiang, and Y. Cui, "The synergetic effect of lithium polysulfide and lithium nitrate to prevent lithium dendrite growth," *Nature Communications*, vol. 6, p. 7436.

[8] B. Scrosati and J. Garche, "Lithium batteries: Status, prospects and future," *Journal of Power Sources*, vol. 195, no. 9, pp. 2419 – 2430, 2010.

[9] A. Manthiram, Y. Fu, S.-H. Chung, C. Zu, and Y.-S. Su, "Rechargeable lithium-sulfur batteries," *Chemical Reviews*, vol. 114, no. 23, pp. 11 751–11 787, 2014.

[10] P. Barai, A. Mistry, and P. P. Mukherjee, "Poromechanical effect in the lithiumsulfur battery cathode," *Extreme Mechanics Letters*, vol. 9, pp. 359 – 370, 2016.

[11] J. Gao, M. A. Lowe, Y. Kiya, and H. D. Abrua, "Effects of liquid electrolytes on the chargedischarge performance of rechargeable lithium/sulfur batteries: Electrochemical and in-situ x-ray absorption spectroscopic studies," *The Journal of Physical Chemistry C*, vol. 115, no. 50, pp. 25 132–25 137, 2011.

[12] S. S. Zhang, "Liquid electrolyte lithium/sulfur battery: fundamental chemistry, problems, and solutions," *Journal of Power Sources*, vol. 231, pp. 153–162, 2013.

[13] Y. Yin, S. Xin, Y. Guo, and L. Wan, "Lithium sulfur batteries: Electrochemistry, materials, and prospects," *Angewandte Chemie International Edition*, vol. 52, no. 50, pp. 13 186–13 200.

[14] S. S. Zhang, "Improved cyclability of liquid electrolyte lithium/sulfur batteries by optimizing electrolyte/sulfur ratio," *Energies*, vol. 5, no. 12, pp. 5190–5197, 2012.

[15] L. Li, T. A. Pascal, J. G. Connell, F. Y. Fan, S. M. Meckler, L. Ma, Y.-M. Chiang, D. Prendergast, and B. A. Helms, "Molecular understanding of polyelectrolyte binders that actively regulate ion transport in sulfur cathodes," *Nature communications*, vol. 8, no. 1, p. 2277, December 2017.

[16] A. Manthiram, Y. Fu, and Y.-S. Su, "Challenges and prospects of lithiumsulfur batteries," *Accounts of Chemical Research*, vol. 46, no. 5, pp. 1125–1134, 2013, pMID: 23095063. [Online]. Available: https://doi.org/10.1021/ar300179v

[17] P. R. Griffiths and J. A. De Haseth, *Fourier transform infrared spectrometry*. John Wiley & Sons, 2007, vol. 171.

[18] H.-H. Perkampus, *UV-VIS Spectroscopy and its Applications*. Springer Science & Business Media, 2013.

[19] J. F. Watts, "X-ray photoelectron spectroscopy," *Surface science techniques*, pp. 5–23, 1994.

[20] J. I. Goldstein, D. E. Newbury, J. R. Michael, N. W. Ritchie, J. H. J. Scott, and D. C. Joy, *Scanning electron microscopy and X-ray microanalysis*. Springer, 2017.

[21] B. E. Warren, *X-ray Diffraction*. Courier Corporation, 1969.

[22] H. Friebolin and J. K. Becconsall, *Basic one-and two-dimensional NMR spectroscopy*. VCH Weinheim, 1993.

[23] S. Zhang, K. Ueno, K. Dokko, and M. Watanabe, "Recent advances in electrolytes for lithiumsulfur batteries," *Advanced Energy Materials*, vol. 5, no. 16.

[24] M. M. Cerda, M. D. Hammers, M. S. Earp, L. N. Zakharov, and M. D. Pluth, "Applications of synthetic organic tetrasulfides as $h_2s$ donors," *Organic letters*, vol. 19, no. 9, pp. 2314–2317, 2017.

[25] B. D. Vineyard, "Versatility and the mechanism of the n-butyl-amine-catalyzed reaction of thiols with sulfur," *The Journal of Organic Chemistry*, vol. 32, no. 12, pp. 3833–3836, 1967.

[26] P. Das, S. Ray, A. Bhaumik, B. Banerjee, and C. Mukhopadhyay, "Cubic $ag_2o$ nanoparticle incorporated mesoporous silica with large bottle-neck like mesopores for the aerobic oxidative synthesis of disulfide," *RSC Advances*, vol. 5, no. 9, pp. 6323–6331, 2015.

[27] M. K. Denk, "The variable strength of the sulfur–sulfur bond: 78 to 41 kcal–g3, cbs-q, and dft bond energies of sulfur (s8) and disulfanes xssx (x= h, f, cl, ch3, cn, nh2, oh, sh)," *European journal of inorganic chemistry*, vol. 2009, no. 10, pp. 1358–1368, 2009.

[28] M. Wu, Y. Cui, A. Bhargav, Y. Losovyj, A. Siegel, M. Agarwal, Y. Ma, and Y. Fu, "Organotrisulfide: A high capacity cathode material for rechargeable lithium batteries," *Angewandte Chemie International Edition*, vol. 55, no. 34, pp. 10 027–10 031, 2016.

[29] W. Guo, Z. D. Wawrzyniakowski, M. M. Cerda, A. Bhargav, M. D. Pluth, Y. Ma, and Y. Fu, "Bis (aryl) tetrasulfides as cathode materials for rechargeable lithium batteries," *Chemistry-A European Journal*, vol. 23, no. 67, pp. 16 941–16 947, 2017.

[30] K. G. Gallagher, S. E. Trask, C. Bauer, T. Woehrle, S. F. Lux, M. Tschech, P. Lamp, B. J. Polzin, S. Ha, B. Long *et al.*, "Optimizing areal capacities through understanding the limitations of lithium-ion electrodes," *Journal of The Electrochemical Society*, vol. 163, no. 2, pp. A138–A149, 2016.

[31] L. Nyholm, G. Nyström, A. Mihranyan, and M. Strømme, "Toward flexible polymer and paper-based energy storage devices," *Advanced Materials*, vol. 23, no. 33, pp. 3751–3769, 2011.

[32] L. Hu, M. Pasta, F. La Mantia, L. Cui, S. Jeong, H. D. Deshazer, J. W. Choi, S. M. Han, and Y. Cui, "Stretchable, porous, and conductive energy textiles," *Nano letters*, vol. 10, no. 2, pp. 708–714, 2010.

[33] Y. Liang, Z. Tao, and J. Chen, "Organic electrode materials for rechargeable lithium batteries," *Advanced Energy Materials*, vol. 2, no. 7, pp. 742–769, 2012.

[34] B. K. Bordoloi and E. M. Pearce, "Oligomeric alkenyl polysulfide: Synthesis and characterization by nmr analysis," *Journal of Polymer Science Part A: Polymer Chemistry*, vol. 16, no. 12, pp. 3293–3300, 1978.

[35] P. Walker Jr, J. Rakszawski, and A. Amington, "Determination of graphitic and amorphous carbon," Pennsylvania State Univ., State College, Tech. Rep., 1955.